**DOI 10.31489/2023No4/6-16**

**UDC 538.913; 620.1**

# INVESTIGATION THE MAGNETIC PROPERTIES OF $Cs_yCo_{1-0.5y}Fe_2O_4$ NANOPARTICLES AT LOW MOLAR RATIO VARIATION

Tareq M.H., Lafta Sadeq H., Hussain Wafaa A.

Applied Science Department, University of Technology, Iraq, Baghdad

*The effect of substitution ferrite by previously not used elements to control magnetic properties is of great interest to researchers. This study illustrates the effect of low substitution of Cs, with molar ratios of y of 0.0, 0.05, 0.15, and 0.25 on the structural and magnetic properties of $Cs_yCo_{1-0.5y}Fe_2O_4$ nanoparticles. The synthesizing method was the co-precipitation method. The metal chlorides were used to perform the reaction in the distilled water using NaOH to reach a pH of 10. The X-ray diffraction, Field Emission Scanning Electron Microscopy, Electron Dispersive X-ray and Vibrating Sample Magnetometry analyses were conducted for all samples. All samples had the patterns of the spinel structure coincide to a high degree with the Co ferrite pattern. There was a general increase in the lattice constant with the increase in the Cs content, while the crystallite size decreased from about 18 to 12.2 nm as the molar ratio increased from 0 to 0.25. The Electron Microscopy investigation showed that all samples owing spherical nanoparticles with no other shapes. The average particle sizes were between 40 to 60 nm, which increased $Cs^{1+}$ content. The magnetic parameters mainly showed a relatively high coercivity (wide loops) and a decrease in magnetization saturation (down to 50.43 emu/g), crystalline anisotropic constant, and the squareness ratio.*

**Keywords:** Cesium Cobalt Ferrite, Structural properties, Hysteresis loop, Nanoparticles, Magnetization.

## 1. Introduction

Spinel ferrite nanoparticles of the composition ($MFe_2O_4$) have attracted considerable interest due to their unique chemical and physical properties. Cesium Cobalt ferrites are hard ferrite materials because of their excellent chemical stability and mechanical hardness. Cobalt ferrite is an important material because of its excellent properties, such as moderate saturation magnetization, large coercivity, large magneto-crystalline anisotropy, high Curie temperature, high electrical resistivity, and high stability [1].

Ferrites are prepared by various methods including such as sol-gel, hydrothermal, microemulsion, thermal decomposition, co-precipitation methods, hydrothermal and solvothermal [2], etc. The main difficulty during synthesis by these methods is to control the particle size and shape in addition to the purity of the product phase. Among these methods, is the co-precipitation method, which has different advantages like its production of inexpensive nanomaterials, less energy requirement, uniformity in particle size, easy experimental conditions adjusting, and easy removal of soluble impurities [3]. Changing the experimental conditions in the co-precipitation synthesis may lead to tailoring the morphological, magnetic, electric, and optical behavior of the produced particles [4]. In the co-precipitation method, nanoparticles are synthesized by adjusting the concentration of precipitating agents to produce stable nanoparticles. On the other hand, the precipitating agents play an important role in determining the various properties of materials. The strength of bases strongly influences the rate of reaction. NaOH has ionic bonding whereas $NH_4OH$ has covalent bonding due to which the reaction rate with other ions could be different [5]. It may lead to different growth and crystallization rates, which could affect the various properties of the synthesized material.

The physical properties of ferrite may be controlled by alteration of the particle size, shape, cation distribution in their lattices, and/or composition [6]. The wide range of each property determines the application of ferrite. These applications extend to various fields including the automobile industry, ultrasonic generation and detection, magneto-restrictive filters, sensors, transformers, and high-density recording industries as well as in the medical industry [7].

Various literature deals with synthesizing Co ferrite by the co-precipitation method, but nearly no study deals with Co ferrite properties due to substitution by Cs. Houshiar et al. [7], prepared Co ferrite nanoparticles by co-precipitation method where metal chlorides as starting materials and sodium hydroxide are used as a precipitating agent. The obtained sample was heated at 600$^o$C for 10h. X-ray analysis reported

that the crystallite size of the prepared sample was 49.5nm. Vibrating Sample Magnetometry (VSM) study showed that the saturation magnetization ($M_s$) of the synthesized sample was 55.8 emu/g and coercivity ($H_c$) was 850 Oe. Surface morphology was studied by SEM and by Transmission Electron Microscopy (TEM) images. Devi Gole et al. [8], synthesized Co ferrite with different pH via the co-precipitation method. The X-ray diffraction (XRD) pattern of this study investigated the lattice parameter varied from 8.4057 to 8.3754Å for different pH and crystallite size varied in the range of 328 to 351Å. The in-vitro antibacterial activity reported that cobalt ferrite at pH of 7 showed the highest antibacterial effects and cobalt ferrite at pH of 8 showed antifungal effects. Kim et al., [9] fabricated cobalt ferrite by co-precipitation technique using chlorides are precursors and sodium hydroxide as a precipitating agent. The authors reported the structural, magnetic, and Mossbauer studies of obtained samples. X-ray patterns of prepared samples have been taken at various temperatures. XRD analysis revealed that the average particle size increased with increasing temperature. The morphology of samples was carried out by TEM images.

Ferrites, especially Cs ferrite and Co ferrite, have promising applications in various fields of magnetics, electronics, and biomedical sciences [5]. Alteration and controlling magnetic properties is regarded as a great challenge aim for most researchers in the field of magnetic materials. The object of this work is to study the effect of variation Cs content, at a low ratio, on the $CsyCo_{1-0.5y}Fe_2O_4$ ferrite structural and magnetic properties, prepared by the Co-precipitation route. To the best of the authors' knowledge, it is the first time to synthesize such nanoparticles of ferrite and investigate their properties.

## 2. Experimental part

The starting materials for synthesizing the $Cs_yCo_{1-0.5y}Fe_2O_4$ nanoparticles were cobalt di-chloride $CoCl_2$, cesium di-chloride ($CsCl_2$), iron tri-chloride ($FeCl_3$), sodium hydroxide (NaOH) and distilled water. Preparation of the $Cs_yCo_{1-0.5y}Fe_2O_4$ by co-precipitation wet method involved weighting of the mentioned salts to verify the molar ratios (y) of 0.0, 0.05, 0.15, and 0.25. The weights of the salts, for each sample (molar-ratio) are shown in Table 1.

**Table 1.** The weights of the precursors (metal salts) at each molar ratio (y).

| Sample | y | Weight of CsCl (g) (M=168.36 g/mol) | Weight of $CoCl_2.6H_2O$ (g) (M=**237.9309**g/mol) | Weight of $FeCl_3$ (g) (M=162.2 g/mol) |
|---|---|---|---|---|
| S1 | 0 | 0 | 2.3793 | 3.2440 |
| S2 | 0.05 | 0.16835 | 4.6396 | 6.488 |
| S3 | 0.15 | 0.5051 | 4.4017 | 6.488 |
| S4 | 0.25 | 0.8418 | 4.1638 | 6.488 |

The next step is mixing the salts together with 150ml of distilled water under strong stirring to prepare a clear precursor solution. Then, adding NaOH dropwise to the solution up to make pH of 10, associated continuing with magnetic stirring to ensure the solution homogeneity. After that, the suspension was heated at 80 for 1h. This is followed by washing the suspension with distilled water several times to remove soluble impurities of salts. The next step is drying the suspension with centrifugal tubes and heating it in an oven at 80°C. Finally, a heat treatment for 4h at 250°C was conducted to accomplish the calcination. The synthesizing steps are shown in the block diagram in Fig.1.

The resulting nanoparticles for the four samples were subjected to different structural and magnetic analyses, which were XRD Shimadzu 6000 as the x-ray diffractometer, Scanning Electron Microscope (SEM) MIRA3 TESCAN as the scanning electron microscope, ALPHA II Compact FTIR Spectrometer as the Fourier Transform Infrared Spectroscopy (FTIR) device, and MDK as the VSM device at 300K temperature with an applied magnetic field 30.000 Oe.

.

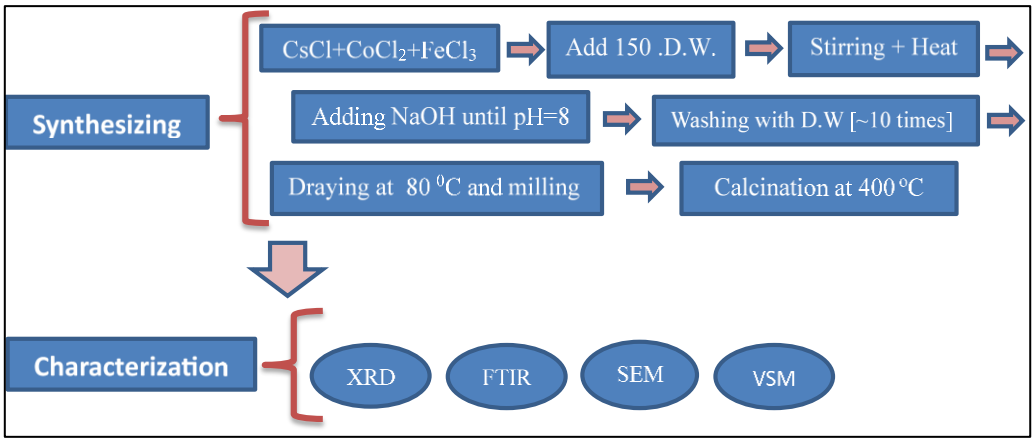


**Fig.1.** The steps for synthesizing the Cesium Cobalt Ferrite $Cs_yCo_{1-0.5y}Fe_2O_4$ nanoparticles by co-precipitation method and their characterization.

## 3. Results and discussion

### 3.1. Structure Properties

Studying the XRD of the prepared nanoparticles reveals the phase and crystallinity of the nanoparticles. The XRD patterns of $Cs_yCo_{1-0.5y}Fe_2O_4$ ferrite for y=0, 0.05, 0.15, and 0.25 are shown in Fig. (2). The resulting patterns reveal that the synthesized nanoparticles have a face-centered cubic spinel structure with good crystallinity. The common Bragg diffraction peaks for all samples were at 2Θ of 30.15°, 35.52°, 43.15°, 53.63°, 57.04°, and 62.61°, which correspond to the reflection planes (220), (311), (222), (400), (422), (511), and (440), respectively. These peaks are in agreement with the XRD pattern of cobalt ferrite (JCPDS card No. 221086). One can note a small shift in the peak of the (311) planes to the lower 2Θ values due to the substitution of $Co^{2+}$ by $Cs^{1+}$ where the latter has a larger ionic radius (170pm) than the former (79pm) [10]. The calculated data are shown in Table 2. Finally, the peaks around 25° and 33° mainly related to the formation of a small quantity of α-$Fe_2O_3$, where these peaks coincide with its (012) and (104) plane [11]. Hematite, α-$Fe_2O_3$ phase, is usually formed during synthesizing ferrite under un-optimized conditions [12].

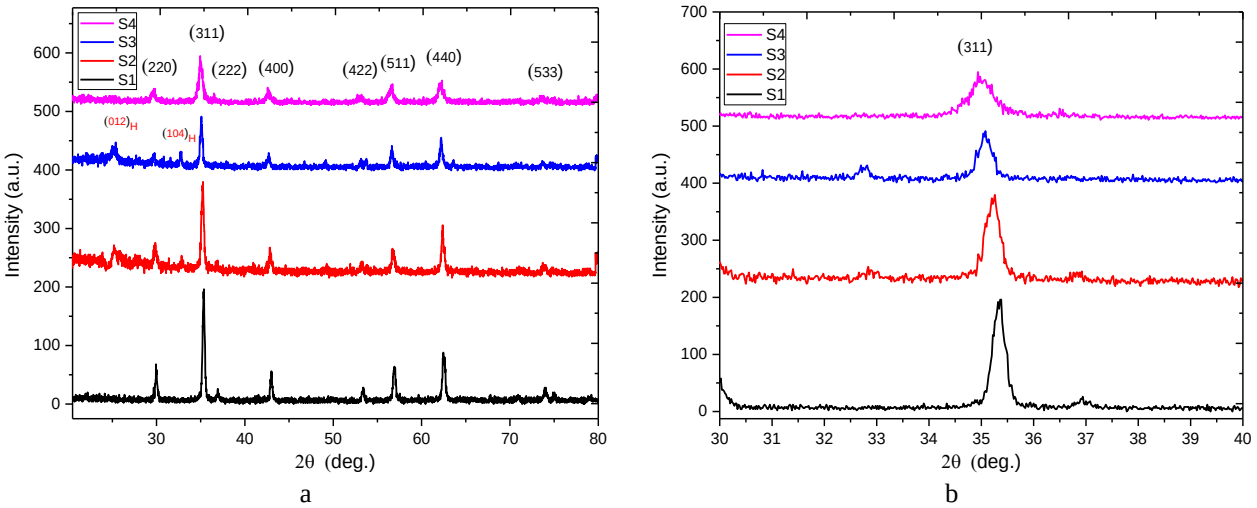


**Fig.2.** (a) The XRD patterns of the synthesized $Cs_yCo_{1-0.5y}Fe_2O_4$ ferrite nanoparticles by co-precipitation method, (b) The peak shifts of the planes (311) for the four samples.

The following reactions are suggested to synthesize the $Cs_yCo_{1-0.5y}Fe_2O_4$ ferrite at the molar ratios y of 0, 0.05, 0.15, and 0.25 respectively:

a) $CoCl_2.6H2o + 2FeCl_3 + 8NaOH \rightarrow CoFe_{2.0}O_4 + 8NaCl + 4H_2O$

b) $2CsCl + 39CoCl_2 + 80FeCl_3 + 320NaOH \rightarrow 40Cs_{0.05}Co_{0.975}Fe_{2.0}O_4 + 320NaCl + 160H_2O$

c) $6CsCl + 37CoCl_2 + 80FeCl_3 + 320NaOH \rightarrow 40Cs_{0.15}Co_{0.925}Fe_{2.0}O_4 + 320NaCl + 160H_2O$

d) $10CsCl + 35CoCl_2 + 80FeCl_3 + 320NaOH \rightarrow 40Cs_{0.25}Co_{0.875}Fe_{2.0}O_4 + 320NaCl + 160H_2O$

The average crystallite size D was calculated by the Scherrer formula as in eq. (1) [11]:

$$D = 0.9\,\lambda/\beta\cos\theta \quad (1)$$

where β is the full width at half maximum of the for the planes (311), λ is the wavelength of x-rays (1.5406Å), and θ is the diffraction angle. All the calculated average crystallite sizes were in the nanometer range.

The crystallite size shows a clear reduction in its value as the molar ratio increases as shown in Table 2, where it dropped from about 18.1nm to about 12.2nm as the molar ratio increases from 0.05 to 0.25. This reduction may be related to the increase of nucleation rate compared to growth rate, i.e., increasing Cs content will improve the nucleation rate and subsequently reduce the crystallite size.

The dislocation density ($d_D$) is proportion inversely to the crystallite size, as given in eq. (2) [12].

$$d_D = 1/D^2 \quad (2)$$

This equation explains the reason behind the increasing dislocation density as in Table 2. The lattice constant (a) for the spinel structure was calculated by the following formula [13]:

$$a = d\,(h^2 + k^2 + l^2)^{1/2} \quad (3)$$

$$d = n\,\lambda/\sin\theta \quad (4)$$

where h, k, and l, are the Miller indices of crystal planes. The calculated lattice constants (a) values were generally increased as the molar ratio increased.

**Table 2.** The effect of Cs content on some structural parameters for S1, S2, S3, and S3. crystallite size D, dislocation density ($d_D$), lattice constants (a), X-ray density ($\rho_{XRD}$), The hopping lengths for A-site ($L_A$) and B-site ($L_B$), and The tetrahedral ($r_A$) ionic radii and octahedral ionic radii ($r_B$)

| Sample | D (nm) | $d_{D\times10^{-3}}$ ($nm^{-2}$) | a (nm) | $\rho_{XRD}$ ($g/cm^3$) | $L_A$ (nm) | $L_B$ (nm) | $r_A$ (nm) | $r_B$ nm |
|---|---|---|---|---|---|---|---|---|
| S1 | 18.12 | 3.044 | 0.840 | 5.24 | 0.3641 | 0.2973 | 0.047 | 0.0752 |
| S2 | 14.98 | 4.45 | 0.838 | 5.42 | 0.3629 | 0.2962 | 0.046 | 0.0745 |
| S3 | 12.62 | 6.27 | 0.848 | 5.45 | 0.3671 | 0.2998 | 0.048 | 0.0770 |
| S4 | 12.27 | 6.64 | 0.841 | 5.83 | 0.3637 | 0.2969 | 0.049 | 0.0750 |

The calculated data are shown in Table 2. As $Cs^{1+}$ content increases and as $Cs^{+1}$ has a larger ionic radius than $Co^{2+}$ this will produce an increase in the calculated lattice constants (a). The measured lattice parameter of sample S1 is comparable to the bulk one of Co ferrite (0.838) [14] where the difference may be related to the low temperature of the preparation. The nanoparticle XRD density (ρ) was calculated by eq. (5) depending on the lattice constant and molecular mass (M). The x-ray density can be calculated using the relation [15]:

$$\rho_{XRD} = 8M/N_A\,a^3 \quad (5)$$

where $N_A$ is the Avogadro number and M is the molecular weight of each structure. The $\rho_{XRD}$ values for the 4 composition nanoparticles are given in Table 2.

The $\rho_{XRD}$ increases as the molar ratio (Cs content) increases despite the expansion in the lattice constant because of the molecular weight increase is more effective than the lattice constant expansion.

The structural parameters such as the hopping lengths for A-site ($L_A$) and B-site ($L_B$) were calculated using standard equations (6) and (7), and the ionic radii ($r_A$ and $r_B$) were determined considering the oxygen positional parameter 'μ' with the standard value of 0.0375 nm and using the radius of oxygen anions $r_o$ of 0.135nm [16]. The tetrahedral ionic radii (A-site) and octahedral ionic radii (B-site) were determined by equations (8) and (9), respectively [17].

$$L_A = a\sqrt{3}/4 \quad (6)$$

$$L_B = a\sqrt{2}/4 \quad (7)$$

.

$$r_A = \left(\mu - \frac{1}{4}\right)\sqrt{3} - r_o \quad (8)$$

$$r_B = \left(\frac{5}{8} - \mu\right)a - r_o \quad (9)$$

The calculated values of the previous parameters, $L_A$, $L_B$, $r_A$, and $r_B$ are given in Table 3. These parameters are raised as the Cs content is increased. In other words, they follow the lattice constant and so their behaviors follow the lattice constant behavior [18]. One may deduce that the tetrahedral substitution has a main effect on the lattice constant value.

### 3.2 The FTIR analysis

Fig.3 illustrates the FTIR spectra of the prepared samples. All samples showed obvious bands below 700cm$^{-1}$, as magnified in the inset Figure, while they showed a low absorption from 700cm$^{-1}$ to 3900cm$^{-1}$ at room temperature. This may be related to the high strength of the ferrite bond due to the ionic nature of the metal-oxygen bond and the nature of the stretching vibration mode**.** The presence of such ferrite characteristic bands refers to the cubic spinel structure and completion of the chemical reaction [19].

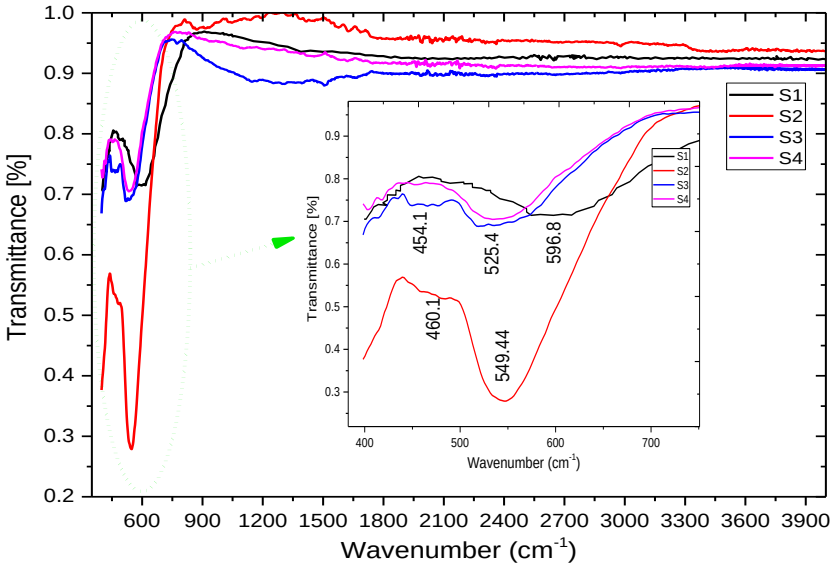


**Fig.3.** FTIR spectra of the synthesized $CsyCo_{1-0.5y}Fe_2O_4$ nanoparticles at 0.0, 0.05, 0.15, and 0.25 for S1, S2, S3, and S3 respectively.

The band around 596cm$^{-1}$, the higher wavenumber, is associated with the stretching mode of the bond of metal at tetrahedral sites and oxygen anion ($Fe^{3+}$–$O^{2-}$ bond), and it is commonly denoted by v1 [20]. On the other hand, the v2-lowest band is observed lower than 500cm$^{-1}$, which results from the octahedral–metal stretching ($M^{2+}$–$O^{2-}$ bond M Is Co or Cs). The v2 band in this study, lower wavenumber, is observed as a strong absorption band between 400 cm$^{-1}$ and 500 cm$^{-1}$ and may extend to values lower than 400 cm$^{-1}$[21].

The $Co^{2+}$ cations generally occupy octahedral sites, whereas $Fe^{3+}$ cations occupy mostly both octahedral and tetrahedral sites. The reason behind the difference in the tetrahedral and octahedral sites is basically associated with the lengths of these two site bond lengths. The precise observation in the inset Figure indicates that there is a general shift in the v1 band to the lower wavenumber as the Cs content increases, while the v2 band exhibits no clear shift. This, in turn, indicates that Cs may mainly occupy the tetrahedral sites rather than octahedral sites. One can observe there is no organic, commonly higher than 2300 cm$^{-1}$[22], or inorganic band or peak that can be related to any impurity or undesirable phase. This perhaps supports the precise synthesizing procedure that was followed. No band around 3410 cm$^{-1}$, which is related to the metal-hydroxide bond [21], is not observed. A weak peak around 1500 cm$^{-1}$ may be related to the symmetric and asymmetric stretching vibration of $CO_2$ molecules in the environment of the test or adsorbed on the particle surfaces [21].

### 3.3. The SEM analysis

The SEM images of the nanoparticles for all samples are given in Fig.4. All samples of $Cs_yCo_{1-0.5y}Fe_2O_4$ (y=0, 0.05, 0.15, 0.25) showed homogeneous spherical nanoparticles without any other observed shape or exotic morphologies. All particle sizes are lower than 100nm as measured by the scale bar. The SEM images substantiate a clear agglomeration. The agglomeration occurred due to surface interaction due to nanosize and magnetic interaction between magnetic nanoparticles [23]. This interaction decreases with increasing cesium concentration in the cobalt ferrite nanoparticles as for other cations.

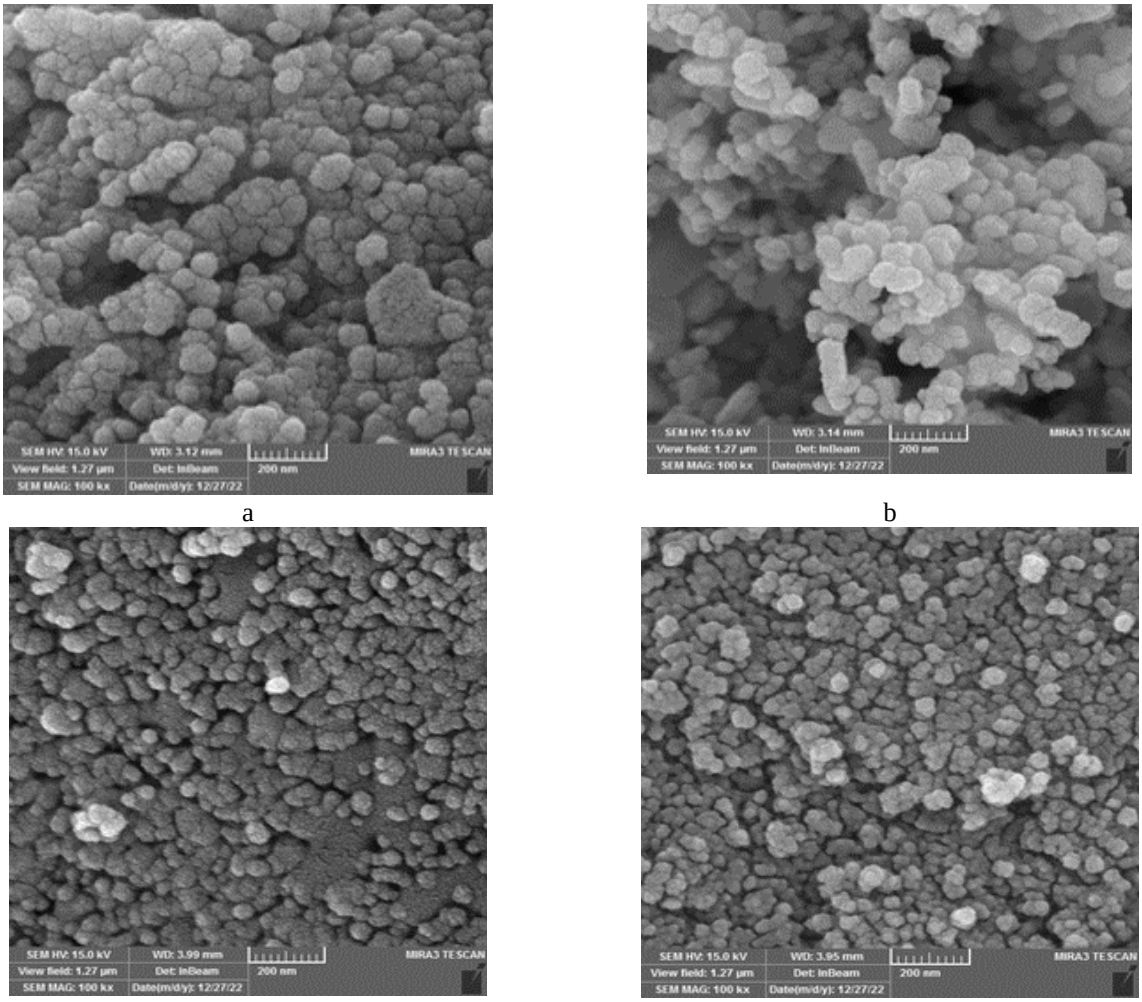


**Fig.4.** SEM images of $CsyCo_{1-0.5y}Fe_2O_4$ samples. (a) sample S1, (b) sample S2, (c) sample S3 and (d) sample S4.

In Fig.5, the particle distributions for the 4 samples are given. The minimum particle size is about 15nm, while it extends to more than 100nm. Most particle sizes are found in the range (40-60) nm. As the molar ratio (y) increases, there is a decrease in the average particle size. This decrease can be attributed to that the presence of $Cs^{1+}$ improves the nucleation rate and, in turn, increases the nucleation centers (seeds) at the expense of single-particle growth [24]. This result is in agreement with the results of crystallite size mentioned previously. In the same context, one can conclude that each particle has more than one crystal.

The elemental composition of samples was carried out by Energy-dispersive X-ray spectroscopy (EDX). Fig.6 shows EDX spectra for all synthesized cesium-substituted cobalt ferrite nanoparticles, which clearly indicates the presence of Co, Cs, O, and Fe elemental corresponding peaks. No presence of any other elemental impurity peak was observed in the EDX spectrum which refers to good choosing synthesizing and measuring conditions. The elemental compositions of all elements for the prepared samples are shown in the inset Tables in the spectra. This result points to obtaining a well-matched atomic ratio of all elements (Co, Cs, O, and Fe) with the expected stoichiometric proportion of elements in the synthesized nanoparticle. The appearance of carbon in the spectra is related to the use of carbon tape for conducting the test.

.

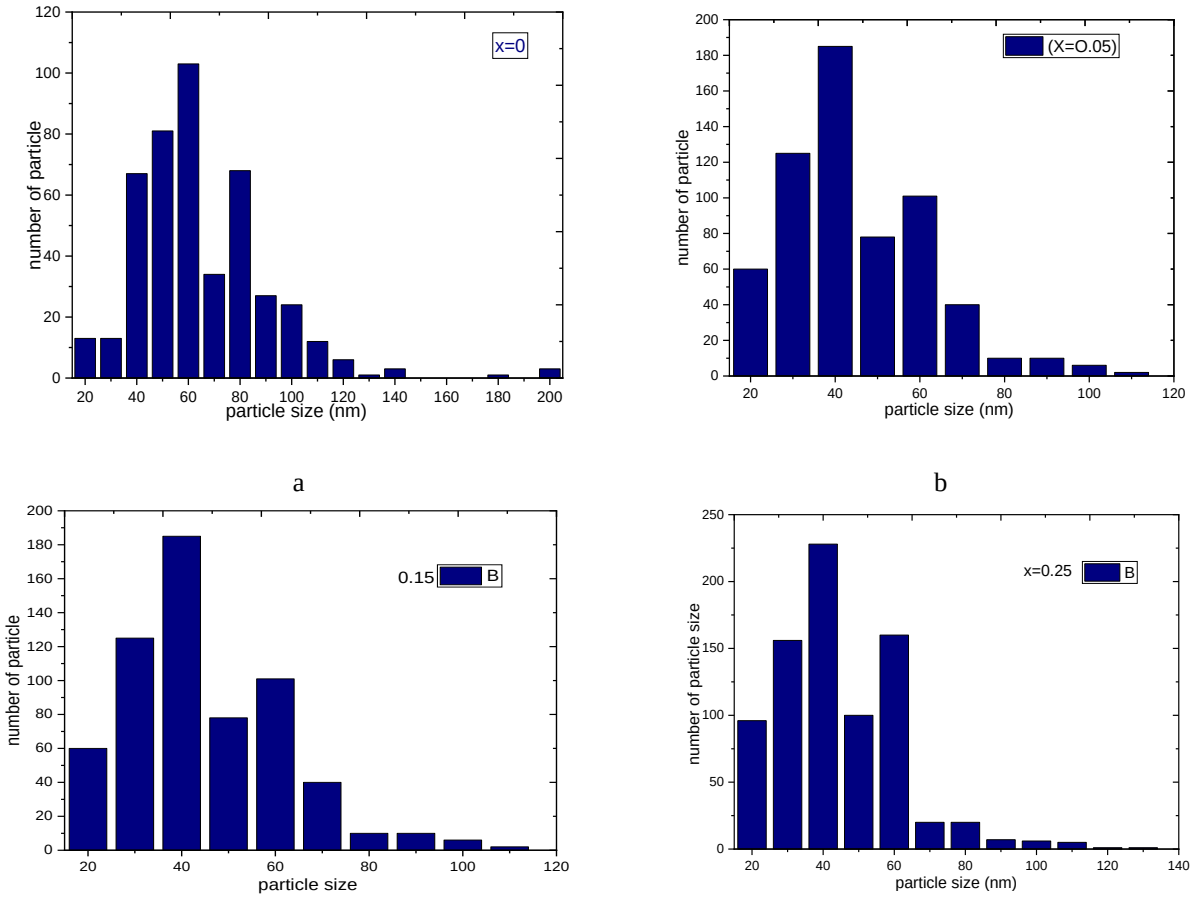


**Fig.5.** The particle size distributions, as measured from the SEM images, for the samples: (a) - sample S1, (b) - sample S2, (c) - sample S3 and (d) s- ample S4.

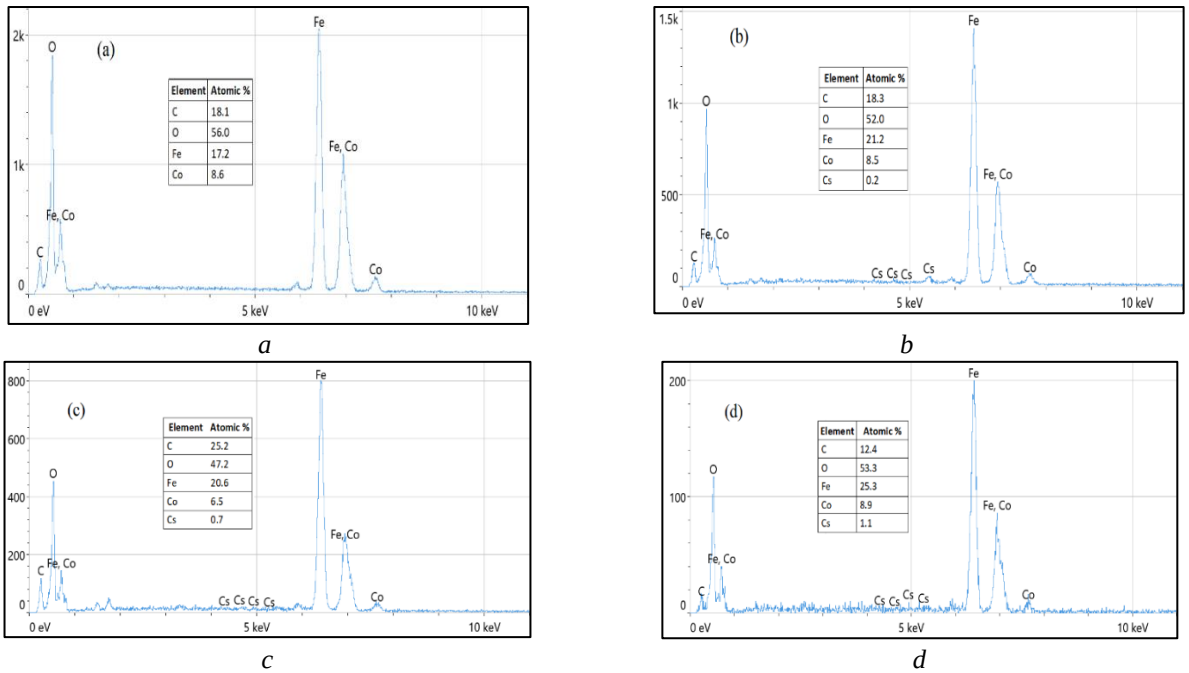


**Fig.6.** The SEM-EDX spectra for the prepared $CsyCo_{1-0.5y}Fe_2O_4$ samples, (a) for y=0, (b) for y=0.05, (c) for y=0.15 and (d) for y=0.25.

### 3.4. Magnetic hysteresis loops analysis

Fig.7 shows the Magnetic hysteresis loops of the synthesized nanoparticles as measured by the VSM magnetometer, these loops correspond to the sample s1, s2, s3, and s4. All samples show nearly hard magnetic behavior compared to cesium ferrite [25].

The saturation magnetization ($M_s$) of the samples showed a generally small reduction as the molar ratio (y) raised from 0 to o.25, although the presence of some tolerance of about 5emu/g, as given in Table 3. Despite of that $Cs^{+1}$ has no magnetic moment but substitution by Cs in tetrahedral or octahedral sites. $Co^{2+}$ ions have a strong preference to take the octahedral site [26]. On the other hand, Cs ferrite is an inverse spinel where all the $Cs^{+1}$ ions occupy octahedral sites while $Fe^{3+}$ ions occupy both octahedral sites and tetrahedral sites [27]. So, according to ratios that were mixed, it is believed that Cs ions usually substitute Co ions. Under this context, the degradation of the $M_s$ is believed due to that $Cs^{1+}$ is owing zero magnetic moment and as it substitutes the $Co^{2+}$, which has a magnetic moment, the magnetization was reduced.

The effect of $Fe^{3+}$ cations is eliminated because an equal number of them occupy A-site and B-sites. Some researchers found that the substitution of $Cs^{+1}$ ions at the tetrahedral (A) site replaces magnetic $Fe^{+3}$ ions which causes a decreased magnetic moment at the A-site [27]. Some other researchers explained the degradation of $M_s$ of Co ferrite when substituted by nan-magnetic ions in B-site on the basis of the magnetization of Co ferrite is higher than that nan-magnetic ions ferrite hence, doping by Cs in cobalt ferrite causes a decrease in magnetization [28].

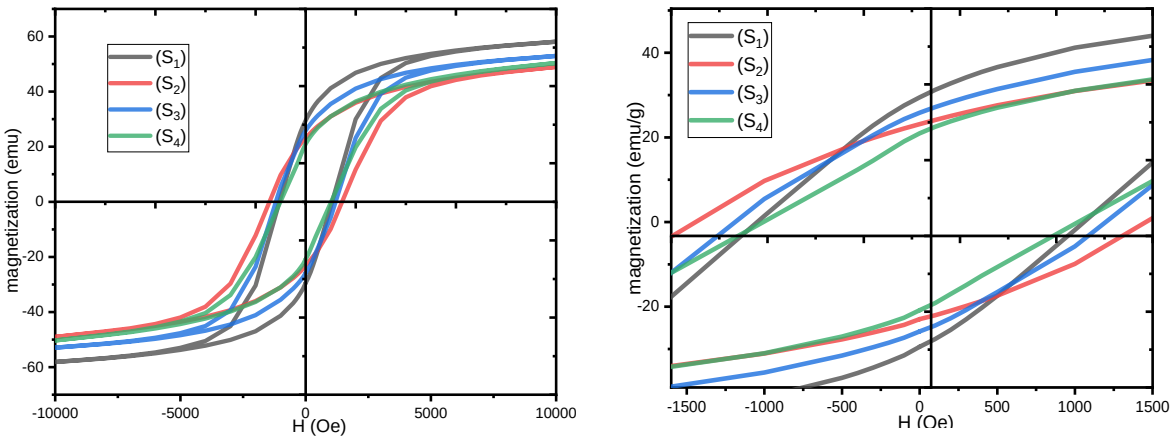


**Fig.7.** The magnetic hysteresis loops of the synthesized $CsyCo_{1-0.5y}Fe_2O_4$ (y= 0, 0.05, 0.15, and 0.25) ferrite: a) full hysteresis loops of the prepared samples; b) a magnification of the origin around to show the details.

**Table 3.** Some magnetic parameters as measured from the magnetic hysteresis loops.

| Sample | $M_s$ (emu/g) | $M_r$ (emu/g) | $H_c$ (Oe) | $M_r/M_s$ | $m_f$ (emu/mol) | $K_{an}$ x $10^3$ (emu.Oe/g) | $m_p$ ($\mu_B$) |
|---|---|---|---|---|---|---|---|
| S1 | 58.075 | 28.87 | 1078.36 | 0.497 | 3.037 | 63.88 | 0.5290 |
| S2 | 48.53 | 19.03 | 1495.32 | 0.454 | 3.986 | 74.06 | 0.3388 |
| S3 | 52.91 | 23.97 | 1196.98 | 0.453 | 4.430 | 57.06 | 0.4396 |
| S4 | 50.43 | 22.04 | 1056.79 | 0.377 | 4.302 | 53.95 | 0.4224 |

In addition to cation distribution and substitution ion type, the $M_s$ of ferrite also depends on the particle size [29]. The Ms dependence on particle size is given in eq. (10) [30, 31]:

$$M_{s/nano} = M_{s/bulk}\ [1 - (B/p_s)] \quad (10)$$

where $M_{s/nano}$ and $M_{s/bulk}$ are the saturation magnetization of nano and bulk materials, respectively, B is a constant, and $p_s$ is the particle size. The remanence magnetization $M_r$ also decreased in general from about 30 emu/g to 20 emu/g). The remanence magnetization usually follows $M_s$ and for the same reasons.

The coercivity ($H_c$) showed a tolerant behavior, where it was increased and then decreased as the molar ratio increased. It is believed the two parameters of composition and the particle size contributed to this behavior. The variation was explained graphically in Fig. (6) in the inset Figure. The mentioned $M_s$ and $H_c$ parameters reveal the ferromagnetic nature of all compositions but not the superparamagnetic one where the main effecting factor here is the particle size.

Some other magnetic parameters are also given in Table 3. The loop squareness ratio ($M_r/M_s$) decreased as the Cs content increased. This behavior depends on the intense surface spin disordering of these nanoparticles and proves the nanoparticles are multidomain ones [32]. For all samples, the $M_r/M_s$ ratio is lower than 0.5, which agrees with the previous result [33]. The crystalline anisotropic constant ($K_{an}$) values are calculated by eq. (11). The $K_{an}$ value is generally minimized as $Cs^{1+}$ content grows. Also, Co ferrite substitution by $Al^{3+}$ showed the same result because of the crystallite size reduction [34].

$$K_{an} = H_c \,.\, M_s/0.98 \tag{11}$$

The magnetic moment per unit formula is calculated by eq. (12). The values decreased as the $Cs^{+1}$ concentration increased. The reduction in $\mu_m$ follows the reduction in $M_s$.

$$m_f = \frac{M \,.\, M_s}{5585} \tag{12}$$

The magnetic moment per particle ($m_p$) was calculated for each sample by the Langevin fitting equation using the Origin Lab program and the values are given in Table 3. This parameter depends on A-B interaction and sharply decreases from (0.5290 to 0.3388 (emu/g) when the value of x is varied from 0 to 0.25. It is also decreased as the $Cs^{1+}$ content increases. The magnetic moment per formula and the magnetic moment per particle are both magnetization saturation dependent, so they follow its behavior.

## 4. Conclusion

Substitutions cations by ions with the oxidation state of +1 like Cs in ferrite is one of the most challenging topics in magnetic material studies. Here, a Co ferrite was chosen to conduct the substitution on its cations satisfying the compositions $CsyCo_{1-0.5y}Fe_2O_4$ with y= 0, 0.05, 0.15, and 0.25. The substitution by $Cs^{1+}$ increases the lattice constant and reduces the crystallite size. A clear shift in the tetrahedral band of the FTIR spectrum supports the substitution occurrence. The magnetization saturation decreased when Co ferrite is substituted by $Cs^{1+}$ cations from about 58 emu/gm down to 50.43 emu/g with low molar ratio variation.

The magnetic moment also decreased as the molar ratio increased. Substitution Co by Cs worked on lowering the average particle sizes as found by the SEM images, but not the particle shape where all samples showed spherical particle shapes. The low Cs substitution did not mainly affect the coercivity where the loops were still wide. There was also a decrease in the crystalline anisotropic constant and the squareness ratio due to such variation in the composition.

## REFERENCES

1 Gore S.K., Jadhav S.S., Jadhav V V. The structural and magnetic properties of dual phase cobalt ferrite. *Scientific Reports*, 2017, Vol.7(1). doi:10.1038/s41598-017-02784-z.

2 Abdel Maksoud M.I., El-Sayyad G.S., Fayad E., et al. Gamma irradiation assisted the sol–gel method for silver modified-nickel molybdate nanoparticles synthesis: Unveiling the antimicrobial, and antibiofilm activities against some pathogenic microbes. *Journal of Inorganic and Organometallic Polymers and Materials*, 2021, Vol. 32(2), pp. 728–740. doi:10.1007/s10904-021-02132-9.

3 Tijerina-Rosa A., Greneche J.M., Fuentes A.F., et al. Partial substitution of cobalt by rare-earths (gd or SM) in cobalt ferrite: Effect on its microstructure and magnetic properties. *Ceramics International*, 2019, 45(17), pp. 22920–22929. doi:10.1016/j.ceramint.2019.07.335.

4 Slimani Y., Almessiere M.A., Hannachi E., Baykal A., Manikandan A., Mumtaz M., Ben Azzouz F. Influence of WO3 nanowires on structural, morphological and flux pinning ability of YBa2Cu3Oy superconductor. *Ceramics International*, 2019, Vol.45, Issue 2, Part A, pp. 2621 – 2628. doi:10.1016/j.ceramint.2018.10.201.

5 Almessiere M.A., Slimani Y., Hannachi E., et al. Impact of DY2O3 nanoparticles additions on the properties of porous YBCO Ceramics. *Journal of Materials Science: Materials in Electronics*, 2019, Vol. 30(19), pp. 17572–17582. doi:10.1007/s10854-019-02106-1.

6 Irfan M., Khan U., Li W., et al. Structural and magnetic properties of fe3ga alloy nanowires: Effect of post annealing treatment. *Journal of Alloys and Compounds*, 2017, Vol. 691, pp. 1–7. doi:10.1016/j.jallcom.2016.08.241.

7 Kounsalye J.S., Kharat P.B., Shisode M.V., et al. Influence of ti4+ ion substitution on structural, electrical and dielectric properties of li0.5fe2.5o4 nanoparticles. *Journal of Materials Science: Materials in Electronics*, 2017, Vol. 28(22), pp. 17254–17261. doi:10.1007/s10854-017-7656-1.

8 Vinayak, V., Khirade P.P., Birajdar S.D., et al. Structural, microstructural, and magnetic studies on magnesium (mg2+)-substituted $CoFe_2O_4$ nanoparticles. *Journal of Superconductivity and Novel Magnetism*, 2016. Vol. 29(4), pp.1025–1032. doi:10.1007/s10948-015-3348-3.

9 Joshi S., Kamble V.B., Kumar M., et al. Nickel substitution induced effects on gas sensing properties of cobalt ferrite nanoparticles. *Journal of Alloys and Compounds*, 2016, Vol.654, pp. 460–466. doi:10.1016/j.jallcom.2015.09.119.

10 Lafta S.H. Evaluation of hematite nanoparticles weak ferromagnetism. *Journal of Superconductivity and Novel Magnetism*, 2020, Vol.33(12), pp. 3765–3772. doi:10.1007/s10948-020-05626-8.

11 Lafta S.H. Hydrothermal temperature influence on magnetic and fmr properties of hematite nanoparticles. *SSRN Electronic Journal*, 2021 [Preprint]. doi:10.2139/ssrn.3989692.

12 Anu K., Hemalatha J. Magnetic and electrical conductivity studies of zinc doped cobalt ferrite nanofluids. *Journal of Molecular Liquids*, 2019, Vol. 284, pp. 445–453. doi:10.1016/j.molliq.2019.04.018.

13 Kurian M., Thankachan S., Nair D.S., et al. Structural, magnetic, and acidic properties of cobalt ferrite nanoparticles synthesised by wet chemical methods. *Journal of Advanced Ceramics*, 2015, Vol.4(3), pp. 199–205. doi:10.1007/s40145-015-0149-x.

14 Patterson A.L. The Scherrer formula for X-ray particle size determination. *Physical Review*, 1939, Vol.56(10), pp. 978–982. doi:10.1103/physrev.56.978.

15 Topkaya R., Baykal A., Demir A. Yafet–Kittel-type magnetic order in Zn-substituted cobalt ferrite nanoparticles with uniaxial anisotropy. *Journal of nanoparticle research*, 2013, Vol.15, pp.1-18. doi:10.1007/s11051-012-1359-6.

16 Demortière A., Panissod P., Pichon B.P., Pourroy G., Guillon D., Donnio B., Bégin-Colin S. Size-dependent properties of magnetic iron oxidenanocrystals. *Nanoscale*, 2011, Vol. 3(1), pp. 225 – 232.

17 Abdel-Mohsen L.H., Lafta S.H., Hashim M.S. Comparing the role of NaOH and NH4OH on structural and magnetic properties of spinel Ba ferrite synthesized by autocombustion method. *Journal of Physics: IOP Conference Series*, 2022, 2322(1), 012081. doi:10.1088/1742-6596/2322/1/012081.

18 Penchal Reddy M., Zhou X., Yann A., Du S., Huang Q., Mohamed A.M.A. Low temperature hydrothermal synthesis, structural investigation and functional properties of Co Mn1−Fe2O4 ($0 \leqslant x \leqslant 1.0$) nanoferrites. *Superlattices and Microstructures*, 2015, Vol.81, pp. 233 – 242.

19 Sagar S., Iqbal N., Maqsood A., Shahid M., Shah N.A., Jamil T., Bassyouni M.I. Fabrication and thermal characteristics of functionalized carbon nanotubes impregnated polydimethylsiloxane nanocomposites. *Journal of Composite Materials*, 2014, Vol. 49(8), pp. 995 – 1006.

20 Kumar H., Singh J.P., Srivastava R.C., Negi P., Agrawal H.M., Asokan K. FTIR and Electrical Study of Dysprosium Doped Cobalt Ferrite Nanoparticles. *Journal of Nanoscience*, 2014, pp.1-10.

21 Ibrahim I., Ali I.O., Salama T.M., Bahgat A., Mohamed M.M. Synthesis of magnetically recyclable spinel ferrite (MFe2O4, M = Zn, Co, Mn) nanocrystals engineered by sol gel-hydrothermal technology: High catalytic performances for nitroarenes reduction. *Applied Catalysis B: Environmental*, 2016, Vol.181, pp. 389 – 402.

22 Gutiérrez L., De la Cueva L., Moros M., Mazarío E., De Bernardo S., De la Fuente J.M., Morales M.P., Salas G. Aggregation effects on the magnetic properties of iron oxide colloids. *Nanotechnology*, 2019, Vol. 30(11), pp.112001.

23 Gbashi K.R., Bahari A., Lafta, S.H. Thin films for nano-electronics applications based on BaCaTiO3–SrZnTiO3 perovskite with Au electrodes. *Applied Physics A*, 2023, 129(5), 350. doi:10.1007/s00339-023-06621-1.

24 Sathya A., Guardia P., Brescia R., Silvestri N., Pugliese G., Nitti S., Manna L., Pellegrino T. CoxFe3–xO4 Nanocubes for Theranostic Applications: Effect of Cobalt Content and Particle Size. *Chemistry of Materials*, 2016, Vol.28(6), pp.1769-1780. doi:10.1021/acs.chemmater.5b04780.

25 Andersen H.L., Saura-Múzquiz M., Granados-Miralles C., Canévet E., Lock N., Christensen M. Crystalline and magnetic structure–property relationship in spinel ferrite nanoparticles. *Nanoscale*, 2018, Vol. 10(31), pp.14902-14914.

26 Gupta M., Randhawa B. Microstructural, magnetic and electric properties of mixed Cs–Zn ferrites prepared by solution combustion method. *Solid State Sciences*, 2012, Vol.14(7), pp.849-856.

27 Rotjanasuworapong K, Lerdwijitjarud W, Sirivat A. Synthesis and Characterization of Fe0.8Mn0.2Fe2O4 Ferrite Nanoparticle with High Saturation Magnetization via the Surfactant Assisted Co-Precipitation. *Nanomaterials*, 2021, Vol.11(4), pp.876. doi:10.3390/nano11040876.

28 Biswal D, Peeples BN, Peeples C, Pradhan AK. Tuning of magnetic properties in cobalt ferrite by varying Fe +2 and Co+2 molar ratios. *Journal of Magnetism and Magnetic Materials*, 2013; 345:1-6. doi:10.1016/j.jmmm.2013.05.052.

29 Lafta SH. Broadband ferromagnetic resonance of non-stoichiometric nano Nickle ferrite with different Ni2+content. *Materials Research Express*, 2019, Vol. 6(4), pp. 046103. doi:10.1088/2053-1591/aafb80

.

30 Lafta SH. The Relation of Crystallite Size and Ni2+ Content to Ferromagnetic Resonance Properties of Nano Nickel Ferrites. *Journal of Magnetics*, 2017, Vol. 22(2), pp.188-195. doi:10.4283/jmag.2017.22.2.188.

31 Jahan N, Uddin MM, Khan MNI, Chowdhury F-U-Z, Hasan MR, Das HN, Hossain M.M. Impact of particle size on the magnetic properties of highly crystalline Yb3+ substituted Ni–Zn nanoferrites. *Journal of Materials Science: Materials in Electronics*, 2021, Vol. 32(12), pp. 6528-16543. doi:10.1007/s10854-021-06209-6.

32 Kumar Y., Shirage P.M. Highest coercivity and considerable saturation magnetization of CoFe2O4 nanoparticles with tunable band gap prepared by thermal decomposition approach. *Journal of Materials Science*, 2017 Vol. 52(9), pp.4840-4851. doi:10.1007/s10853-016-0719-5.

33 Sarmah S., Borah R., Maji P., Ravi S., Bora T. Effect of Al3+ substitution on structural, magnetic and dielectric properties of cobalt ferrite synthesized by sol-gel method and its correlation with cationic distribution. *Physica B: Condensed Matter*, 2022, Vol.639, pp. 414017. doi:10.1016/j.physb.2022.414017.

34 Zhang L., Huang Z, Shao H, Li Y., Zheng H. Effects of γ-Fe2O3 on γ-Fe2O3/Fe3O4 composite magnetic fluid by low-temperature low-vacuum oxidation method. *Materials & Design*, 2016, Vol. 105, pp. 234 – 239. doi:10.1016/j.matdes.2016.05.077.

Article received 28.10.2023
Article accepted 02.11.2023